Published in final edited form as:
NanoImpact. 2018 January 1; 9: 61–71. doi:10.1016/j.impact.2017.10.005.

Evaluating Weathering of Food Packaging Polyethylene-Nano-clay Composites: Release of Nanoparticles and their Impacts

Changseok Han[1,2], **Amy Zhao**[2], **Eunice Varughese**[3], and **E. Sahle-Demessie**[2,*]

[1]Oak Ridge Institute for Science and Education, Oak Ridge TN, 37831, USA

[2]U.S. EPA, Office of Research and Development, National Risk Management Research Laboratory, 26 W. Martin Luther King Drive

[3]U.S. EPA, Office of Research and Development, National Exposure Research Laboratory, 26 W. Martin Luther King Drive

Abstract

Nano-fillers are increasingly incorporated into polymeric materials to improve the mechanical, barrier or other matrix properties of nanocomposites used for consumer and industrial applications. However, over the life cycle, these nanocomposites could degrade due to exposure to environmental conditions, resulting in the release of embedded nanomaterials from the polymer matrix into the environment. This paper presents a rigorous study on the degradation and the release of nanomaterials from food packaging composites. Films of nano-clay-loaded low-density polyethylene (LDPE) composite for food packaging applications were prepared with the spherilene technology and exposed to accelerated weathering of ultraviolet (UV) irradiation or low concentration of ozone at 40 °C. The changes in the structural, surface morphology, chemical and physical properties of the films during accelerated weathering were investigated. Qualitative and quantitative changes in properties of pristine and aged materials and the release of nano-clay proceeded slowly until 130 hr irradiation and then accelerated afterward resulting complete degradation. Although nano-clay increased the stability of LDPE and improved thermal and barrier properties, they accelerated the UV oxidation of LDPE. With increasing exposure to UV, the surface roughness, chemiluminescence index, and carbonyl index of the samples increased while decreasing the intensity of the wide-angle X-ray diffraction pattern. Nano-clay particles with sizes ranging from 2–8 nm were released from UV and ozone weathered composite. The concentrations of released nanoparticles increased with an increase in aging time. Various toxicity tests, including reactive oxygen species generation and cell activity/viability were also performed on the released nano-clay and clay polymer. The released nano-clays basically did not show toxicity. Our combined results demonstrated the degradation properties of nano-clay particle-embedded LDPE composites toxicity of released nano-clay particles to A594 adenocarcinomic human alveolar basal epithelial cells was observed, which will help with future risk based-formulations of exposure.

*Corresponding author. Tel.: +1 (513) 569 7739; fax: +1 (513) 569 7677. sahle-demessie.endalkachew@epa.gov (E. Sahle-Demessie).

Keywords

nanoclay; polymer composite; weathering; nanorelease; nanotoxicity

1. Introduction

Thermoplastic nanocomposites are playing a significant role in the fast growing area of nanotechnology. The volume and types of nanocomposites used for non-structural applications such as packaging are growing (Azeredo, 2009). As compared to the conventional micro and macro fillers, or neat counterparts, low amounts of nano-fillers exhibit superior enhancement of properties of pristine plastics. Engineered nanoparticle (ENPs) are increasingly incorporated in a wide variety of polymeric materials with favorable matrix-filler interaction that resulted in improved physical, chemical, and electrical properties (Chen et al., 2005; Manchado et al., 2005; Kim et al., 2008; Azeredo, 2009). Also, nanoparticles have other “smart” functions such as enzyme immobilization, antimicrobial activities, and recognition of biomolecules. At the same time, the mobility of the nano-fillers in polymer composites is much higher than conventional micro or macro composite fillers because of their comparable time scale of motion with polymer chains (Azeredo, 2009).

Polyethylene (PE, $(C_2H_4)_n$) is a semi-crystalline straight chain polymer and a non-degradable material that is commonly used for food packaging (Mark, 2004). However, requirements for adequate barriers of low density polyethylene (LDPE) to gases and vapors, including improved mechanical properties, have boosted interest in developing new strategies to improve these properties (Mark, 2004; Siročić et al., 2014). Nano-fillers have been widely used in a wide range of applications for food packaging and low concentration of dispersed nano-clay plates suppress polymer crystallization, and they could increase mechanical strength, flame-resistance, and even enhanced transparency while decreasing gas permeability (Giannelis, 1996; Vaia et al., 1996; Lebaron et al., 1999; Morgan, 2007).

For packaging of bread, LDPE-nano-clay composites maintained moisture content and reduced the permeation rate to oxygen gas significantly. The barrier effectiveness increased with increasing nano-clay concentrations while decreasing at higher temperatures (Davoodi and Sourki, 2014). A significant improvement in barrier properties upon an application of a thin nanocomposite coating was reported on various pre-coated structures (Andersson, 2010). Organo-modified montmorillonite (MMT) clays incorporated within LDPE, and the resulting films are characterized regarding their nanostructure, thermal properties, and antimicrobial activity (Dadblin et al., 2008; Shemesh et al., 2015). The LDPE-clay-nanocomposites exhibit excellent and prolonged antimicrobial activity against *Escherichia coli* bacteria, while the composite without the nano-clay lost its antimicrobial function within several days.

This study seeks to investigate the potential release of nanomaterials from polymeric nanocomposites poses real risk. Thermoplastic polymer foil-laminated film as food package films such as LDPE and LDPE-clay by Meal, Ready-to-Eat (MRE) generates a significant amount of waste. LDPE-clay is an organoclay-blended LDPE prepared by in-situ grafting

intercalating in melt to create an intercalated morphology or involved micro-structural diffusion pathway. The blended organoclay limits oxygen and water vapor permeability, resulting in increases of the shelf-life of the packaged contents. Although most studies focused on the intrinsic hazard of discrete nanomaterials and their potential exposure, the prerequisite to any actual exposure is release and transport. The potential release of nanoparticles (NPs) during the use or at the end of their lifetime from their immobilized matrix pose a risk to the environment and human health. It is important to understand a relationship between the inherent characteristics of nanocomposite products and the likelihood of the release and implication of NPs throughout the life-cycle of the goods. To quantify the mass and the form of released NPs from a polymer matrix, we need to understand better the polymer aging processes. Growing scientific evidence that free NPs can cross cellular barriers and that exposure to some of these NPs may lead to oxidative damage and inflammatory reactions. Degraded nanoparticles also have the potential to cause toxicity. Nanomaterials that have been shown to induce toxicity include nano-TiO_2 (Castro et al., 2012; Lewicka et al., 2013), nano-ZnO (He et al., 2014; Lewicka et al., 2013), and carbon-based nanomaterials, such as carbon nanotubes (Schlagenhauf et al., 2015; Guo et al, 2011; Ju et al., 2014). Moreover, increasing use of nanomaterials in volume and types of food packaging may be a cause for concern that the release of NPs from the package would migrate to food or the environment. Predicting structural changes of the polymer matrix and the potential of release of NPs from the polymer composite matrix is needed to develop environmentally benign nanocomposites. This paper presents a study on how accelerated weathering of nanocomposites during service or the end-of-life degrades and assesses the potential risk of releasing embedded NPs. Moreover, the toxicity of NPs released from the nanocomposites was studied.

2. Experimental Section

2.1 Materials

Two types of food packaging materials that are based on LDPE (Packaging Material 1 (PM1) and PM2) were obtained from PerkinElmer Inc. The two samples of LDPE-nanoclay (montmorillonite) composite films (0.5 mm) were produced using film extrusion technique having low (MP1) and high (PM2) clay composition. Additional reference materials were procured from ExxonMobil™ LDPE LD 160AT (Nanocor, Hoffman Estates, IL, USA) and clay cloisite® 20A (BYK-Chemie GmbH, Germany) were used for this study. The size of nanoclay determined by X-ray was 3.16 nm (see Table S1 in the supplemental information). Commercial grade LDPE (ExxonMobil™ LDPE LD 160AT) was used for the preparation of films. The melting flow index (MFI) for the polymer was 0.2 g min^{-1}, with crystalline melting point of 110 °C and density of 0.92 g cm^{-3}. Since the information of nanoclay contents in two samples is not open to public, we estimated it by measuring weights of residues after drying (80 °C for 4 hr) and incineration (650 °C for 12 hr) processes for the samples. The content of each samples was 3.3% for PM1 and 5.4% for PM2 (See supplemental).

2.2. Preparation of the films

The additive-free polymer powders were pelletized using a Rheomex S ¾” type single screw extruder attached to a Haake Rheocord EU 10 V driving unit at 50 rpm and barrel temperatures of 180, 220 and 260 °C, then compression-molded to films at 150 °C using an Agila PE20 hydraulic press (processing conditions: low pressure for 120 s, followed by a high-pressure cycle at 150 bar for 90 s and finally cooling with tap water). The thickness of the obtained films was between 90 and 105 μm. To extract the residual degradation products of low molecular masses, samples were purified with Soxhlet extraction in methanol at 150 °C.

2.3. UV Light Weathering

Accelerated weathering is applied under a controlled and reproducible condition to achieve repeatability. A medium pressure UV lamp was used for this study. Samples were placed on the bench top UV-lamp where the irradiation was 14 mW/m^2. The system allowed direct setting and control of irradiance: 340 nm, 420 nm, 300–400 nm or Lux and direct setting and control of black panel temperature. The relative humidity was measured every 10 s and recorded along with chamber and black panel temperature. The system allows direct setting and control of specimen chamber air temperature. The method used for this study follows ISO-4892-2/2013 method for accelerated aging (Wohlleben, W. and Neubaue N, 2016,). The samples were placed in the center of a borosilicate envelope filter at 40 °C in the presence of air. The aged samples were collected at intervals of 4, 24 and 100 hr.

2.4 Ozone Weathering of Polymer

Polymer films were placed in a temperature controlled stainless pipe (5 cm, ID) placed in a laboratory tube furnace (Carbolite AST series). An ozone generator has a Variac power controller, an ammeter, and a power supply unit to provide the required voltage to generate varying concentrations of ozone. The ozone generator can produce from 3 to 25 g hr^{-1} of ozone. The oxygen source for the ozone generator in the laboratory was bottled oxygen so that the dryness and purity were controlled. The ozone concentration of the gas flow stream was determined using potassium iodide trapping solution method (See supplemental). The generated ozone was humidified by passing a water reservoir and then flowed into the reaction tube. The concentration of ozone was 9–10 mg/L at the inlet of the reaction tube. The aged samples were collected at intervals of 6, 20, 100, 600 and 700 hr. Visual observations and microscopic images of aged films were taken (Supplemental Figure S1). Changes in physical, structural, chemical properties were analyzed with the time of aging by periodic sampling or weathered products.

2.3 Analytical Methods

2.3.1 Thermogravimetric Analysis—Thermogravimetric analysis (TGA) was made as a function of temperature or time under controlled nitrogen atmosphere. This technique is used to characterize how weathering alters sample decomposition. Measurements were used primarily to determine the structural integrity and thermal stability of weathered LDPE composites. Also, TGA is commonly used to establish polymer degradation temperatures, residual solvent levels, absorbed moisture content, and the amount of inorganic filler in the

composite samples. Samples of the polymer (3 to 4 mg) were placed on a TGA aluminum pan. TGA tests were carried out with Perkin Elmer Pyrus 7 TGA under flowing nitrogen stream at 20 ml min^{-1} and a heating ramp rate of 10 °C min^{-1} from 30 to 800 °C. The onset of degradation is characterized by the temperature at which weight changes become detectable. After the initial moisture weight loss process, the TGA profiles of pristine and aged samples typically plateau to some constant weight level until the polymer degradation temperature range was reached.

2.3.2 Chemiluminescence Analysis of aged materials—Photo-oxidation of LDPE generates cabonyl species. According to Russell mechanism, singlet oxygen and excited carbonyl arising from the bimolecular degradation of hydro are produced as a result of luminescence. When an excited carbonyl species returns to the ground state, energy is released as a photon of light. Following this released photon, chemiluminescence (CL), it is possible to measure the degree of oxidation of the sample accurately. A CL analyzer (CLA-FL2, *Tohoku electronics*) was used to measure CL of pristine and aged samples.

2.3.3 X-ray Diffraction Analysis—X-ray diffraction (XRD) was used for the phase identification of crystalline materials and structural changes that include gradual modifications during the weathering process. Crystallinity is closely related to the macroscopic properties of the polymer that are also measured with other techniques. The changes in the phase of LDPE-nano-clay composite exposed to UV or ozone were analyzed using an X-ray diffractometer (Mini Material analyzer, GBC Scientific Equipment Pty Ltd., Australia) using Cu K_α radiation source. Scans were performed over the 2θ range from 5° to 90° at 0.02 step-size and 1-degree min^{-1} scan speed and 1 kW power (λ = 1.54060 Å) of 30 kV and 40 mA. The various phases were predicted on the bases of Joint Committee on Powder Diffraction Standards **(**JCPDS) powder diffraction file cards (ICCD, 1997–2017).

2.3.4 Fourier Transfer Infrared Spectroscopy—Fourier transfer infrared (FTIR) spectroscopy was used to identify changes in surface photo-oxidation in the LDPE by determining the functional groups at surfaces. The surface chemical changes occurring in the LDPE composite films upon exposure to the oxidative environment were investigated using Fourier Transfer Spectrometer (2000 FT-IR SensiR Dicomp, PerkinElmer). Attenuated total reflectance (ATR) method was used to analyze sample surfaces. Surface chemical bonds that absorb UV light of varying frequencies and different functional groups in the LDPE were detected by the absorption of IR at a particular frequency. FTIR also can be used to identify these carbonyl groups such as ketones, carboxylic acids, and aldehydes (Andersson, 2010). Carbonly index (CI), was used as a parameter to monitor the degree of photo-oxidation of polyethylene and has been calculated according to the base-line method (Amin and Scott, 1974) to the absorbance of strong peak due to the asymmetric C-H stretching at 2924 cm^{-1} (Chidambaram and Krishnasamy, 2014). Carbonyl index is the ratio between the absorbance of the carbonyl peak (1712 cm^{-1}) and the absorbance of the -CH_2 groups at 1465 cm^{-1}.

$$Carbonyl\ Index\ \ (CI) = \frac{Absorption\ at\ 1712\ cm^{-1}}{Absorption\ at\ 1465\ cm^{-1}}$$

The CI is given at the ratio of the maximum absorption carbonyl peak and a peak for the internal thickness band.

2.3.5 Atomic Force Microscopic Analysis—Photodegradation of polymeric materials starts at the surface due to higher light absorption and the presence of oxygen and proceeds into the bulk matrix. The changes in thin films of polymeric materials indicate that the weathering affects different properties of the materials. Atomic force microscopy (AFM) is a characterization tool for polymers that is capable of revealing surface structures with superior spatial resolution (Cohen et al., 1994). AFM uses the universal character of repulsive forces between a tip and samples for surface analysis that enables examination of even single polymer molecules without disturbance of their integrity to measure the surface morphology on the atomic scale (Paul et al., 2005). By using AFM, the rearrangement processes of the polymer chains can be measured at the nanoscale. The surface structure of the thin film was observed using an Agilent 5500 AFM/SPM microscope in Tapping mode. The images were obtained and analyzed using Gwyddion software (version 2.12).

2.3.6 Scanning Electron Microscopy—Scanning electron microscopy (SEM) was used to investigate the surface morphological changes during the weathering of LDPE. Low vacuum sputter-gold coating of the sample was to make it electrically conductive and avoid image artifacts. Although the resolution of SEM images may not show the dispersion of nanoparticles in the polymer, it is a valuable tool for investigating morphological changes of the polymer surface such as fractured surface morphology of the films. For the analysis of sample surfaces, a JEOL SEM (JSM6490V) was used at a voltage of 3–5 kV.

2.4 Analysis of Released Nanoparticles

Samples of aged LDPE composite films were weighed and put in a beaker filled with 20 mL distilled water. To accelerate the release of nanomaterials from aged LDPE composite films by providing a severe agitating condition, the beaker was sonicated for 15 min at room temperature. The water samples were collected for further analysis for the presence of micro-polymers and released nanoparticles.

2.4.1 Transmission Electron Microscopy—Transmission electron microscopy (TEM) was used to investigate nano-clay leaching from LDPE-nano-clay samples after UV and O_3 weathering processes. For the analysis, UV and O_3-aged samples for 100 h and 793 hr, respectively, were sonicated using a lab sonicator (Branson 2800, Branson Ultrasonics Co., Danbury, CT, USA) for 30 min. Supernatant was taken and dropped on copper TEM grids (LC352-Cu, Electron Microscopy Sciences). The grids were dried at room temperature before TEM analysis. For the analysis, a high resolution TEM (HR-TEM, JEM-2010F, JEOL, Japan) was operated with a field emission gun at 200 kV.

2.4.2 Inductively Coupled Plasma-Optical Emission Spectrometers (ICP-OES)—Trace concentrations of metals leached from the sonicated polymer films were analyzed using an inductively coupled plasma-optical emission spectrometer (ICP-OES Optima 2100 DV Perkin Elmer Inc., CT, USA). A lower concentration of 18-metals method, from 1.57 to 15.7 mM, was used to calibrate the instrument. The metals analyzed were As, Al, Cd, Cr,

Cu, Fe, Pb, Mg, Mn, K, P, Ni, Na, Si, Zn, Ca, Ag, and Ba. The detection limit was lower than the lowest metal concentration measured, which were within the range of 0.0002 nM (Ca^{2+}) to 0.5 nM (K). For measuring released nanoclays from aged polymer composite, films (2 cm × 2 cm) were submerged in 5 mL deionized water. The samples were then sonicated for 20 min. The films were removed, and the vials containing water with the released materials were put in nitrogen evaporator (N-EVAP, Oranomation). The dried samples were diluted with concentrated HNO_3 (10 wt %) and microwave acid digested following EPA Method 3052 (MARS CEM Co.). Moreover, the initial concentrations of nano-clay in raw LDPE composites of PM1 and PM2 were estimated by placing samples in crucibles in a furnace (Ney® VULCAN 3-550) at 650 °C for 4 hrs. The leftover ash samples were transferred to vials and then diluted with HNO_3 and microwave digested following the same procedure for the ICP sample preparation method.

2.4.3 Fluorescent Analysis for Measurement of Reactive Oxygen Species—The formation of reactive oxygen species (ROS) by nano-clays was studied to investigate the release of clay nanoparticles from the polymer nanocomposites, indirectly. For a measurement of ROS, in particular for singlet oxygen ($^1O_2$), a detection reagent, Singlet Oxygen Sensor Green (SOSG, Molecular Probes, Inc.), was used. First, a stock solution of SOSG (330 μM) was prepared with 33 μL methanol (HPLC grade, Fisher Chemical) and MilliQ grade water. Then, nano-clay samples with different concentrations from 0 to 10 mg L^{-1} were prepared in glass petri dishes (diameter: 60 mm) to estimate the concentration of the quantification of released nano-clay particles from aged polymer composites. The final concentration of SOSG in the samples was 1 μM. For the preparation of an actual sample, 18.0 mg UV aged LDPE nanocomposite for 100 hr was added in 25 mL Milli-Q grade water and then sonicated for 10 min. The supernatant was used for ROS measurement experiments. All prepared samples were exposed to UV in a PELCO UVC3 Cryo chamber (Ted Pella, Inc.). A solution sample of 500 μL was taken from the nano-clay samples every 5 min for 30 min and the intensity of each sample was measured using Trilogy laboratory fluorometer (Turner Designs) with a fluorescein module. As background experiments, fluorescence units (FSU, excitation/emission maxima ~504/525 nm) for dark and UV exposure conditions without nano-clay were measured and subtracted from the FSU values for all nano-clay samples.

2.4.4 Cell culture maintenance & treatment—Human alveolar epithelial cells (A549; CCL-185, ATCC) were cultured in Dulbecco's Modified Eagle Medium (DMEM, Gibco), supplemented with 10% FBS (Hi-Clone), 1% sodium pyruvate (Gibco), and 1% penicillin-streptomycin-neomycin (PSN, Gibco). Cells were grown at 37 °C in a 5% CO_2 atmosphere. Cells were passaged at 70–80% confluency every 2–4 days. For testing, LDPE-nano-clay (composite) and LDPE-clay (polymer) was suspended in culture medium to a final stock solution of 25 mg mL^{-1}. The particle suspensions were sonicated in an ultrasonic bath for 10 min immediately prior to exposure to cells.

2.4.5 Detection of reactive oxygen species (ROS) in cells—Intracellular ROS formation was determined using the dichlorofluorescein (DCF) assay. This assay measures the conversion of H2DCF (2′,7′-dichlodihydrofluorescein, Molecular Probes) to fluorescent

DCF by ROS. For each test, 2×10^4 A549 cells were seeded per well of a 96 well plate in a volume of 200 μL and grown for 1 day. The medium was replaced by 100 μL of 50 μM H2DCFDA in Hank's buffered salt solution (HBSS), and cells were incubated for 60 min at 37 °C and 5% CO_2. Thereafter, the cells were washed with prewarmed HBSS, and exposed to 100 μL of suspended solutions of PM1 or PM2. The peroxinitrite donor 3-morpholinosydnonimine (Sin-1, Sigma-Aldrich) was used as a positive control, as it generates both superoxide anions and nitric oxide that spontaneously form peroxynitrite, a potent oxidant. Fluorescent intensities were measured after 2 h using a fluorescent microplate reader (Becton Dickinson) at an excitation wavelength of 485 nm and an emission wavelength of 528 nm. Fluorescence values were blank-corrected and normalized.

2.4.6 Analysis of cell viability & activity (MTS Assay)—Cell viability was determined using the CellTiter 96 AQueous One solution (Promega) containing 3-(4,5-dimethylthiazol-2-yl)-5-(3-carboxymethoxyphenyl)-2-(4-sulfophenyl)-2H-tetrazolium inner salt [MTS] as the tetrazolium compound and an electron coupling reagent (phenazine ethosulfate; PES). This assay was performed according to manufacturer's instructions, with 8×10^3 A549 cells seeded in 200 μL of complete cell culture medium per well of a 96 well plate and grown for 1 day. Cells were then treated with 200 μL of suspended solution of PM1, PM2, or the positive control $CdSO_4$ (100 μM) for 24 h or 48 h. At the different timepoints, medium containing stimuli was replaced by 120 μL of MTS working solution and incubated for 60 min at 37 °C and 5% CO_2 before the optical density was measured at 490 nm in a microplate reader (Becton Dickinson). Original OD (490) values were blank-corrected.

3. Results and Discussion

3.1 Chemiluminescence

The intensity of the CL signal from a UV irradiated and ozone exposed PM1 and PM2 was determined as a function of time. The CL intensity from aged polymer indicates the excitation of oxidized chemicals due to chemical activation. The structure and additive of nano-clay in the polymer affect the observed patterns of CL response in oxygen at 40 °C (Supplemental Figure S2). The oxidative process was related to the concentration of hydroperoxides, carbonyl groups or of other oxidized structures and terminal groups. The CL and oxidation induction time (OIT) tests are employed to monitor the thermo-oxidative degradation of LDPE film. The CL emission intensity was increased with increasing exposure time. Furthermore, the OIT result suggested that both UV and ozone exposed samples start emission instantly where ozone aging resulted in a much stronger emission intensity. PM2 sample showed higher CL intensity due to the direct oxidation of the clay additives. The rate of oxidative attack is then related to the strength of the signal and the molar mass of radicals formed. Oxidative degradation could be visualized using CL intensity and it varied over the surface of the sample specimen.

3.2 Thermogravimetric Analysis

Thermogravimetric technique was used to measure the thermal stability of pristine PM1 and PM2 samples under the flow of nitrogen. The results of TGA in Figure 1 (A) demonstrates

that slightly higher thermal stability of PM1 sample compared to PM2 based on increased onset decomposition temperature, *T*onset, and the temperature of maximum weight loss rate, *Tpeak*, for nanocomposites. Figure 1 (A) presents the TGA results of PM1 and PM2 samples. As evident from the figure, both samples exhibit single step decomposition over a relatively wide temperature range. The TGA results showed that the onset of thermal degradation for PM2 was similar with a difference of approximately 5 °C compared to PM1 film. The tests suggest that the difference in clay content did not result in a significant change of thermal stability of the two samples. Other studies reported the thermal stability was improved due to the nanoscale dispersion of clay layer and silicate layer in the PE and poly(lactic acid) matrices, respectively (Hinsken et al., 1991; Lin and Yu, 2007). The higher thermal stability could due to the formation of a char in exfoliated nanocomposites which hinders the out-diffusion of the volatile decomposition products, resulting in the decrease of permeability (Moniruzzaman, and Karen, 2006). The degradation patterns for PM1 are shown in Figure 1 (B). Weight loss of the sample was 5 to 7%, which is associated with the loss of water in the first range (30-300 °C). In the second stage between 300 and 450 °C, different degradation patterns were observed for each sample with different UV exposure times. Oxidized parts of samples by UV photo-oxidation started getting decomposed by heating. The sample aged for longer times under UV lost more mass compared to the sample shortly exposed to UV. It indicates the films were photo-oxidized and their thermal stability decreased due to UV irradiation. Then, samples degraded significantly loosing 80 wt% of their mass (mostly LDPE) between 450 and 490 °C. Previous studies have shown that thermal oxidation of polyethylene involves breaking weak link moieties namely, peroxides, carbonyl groups and unsaturated structures. (Singh and Sharma, 2008). After this range, only 3–6% of total mass of samples remained in the pan for TGA analysis. However, UV irradiated PM2 sample displayed thermal stability and no significant changes of degradation were observed under extended UV illumination (Figure 1 (C)), indicating the nano-clay composition in PM2 is higher than PM1. The decomposition of PM2 by heating was a single step process with no mass loss in a range between 300 to 450 °C. TGA and DTG plot shows a significant mass loss was observed around 472 °C.” The decrease in the thermal stability of nano-clay PE was more significant for ozone aged samples shown in Figure S 3(A) and 2(B). Studies have shown that polymers subjected to polluted atmospheres, ozone reacts with polymers at room temperature and form radicals at high rates (Grassie and Scott, 1985). In previous studies, no further improvement in thermal stability was reported above a clay loading of 10 wt% (Kocun et al., 2011). Therefore, the contents of clay nanoparticles in polymers must be carefully optimized to obtain high thermal stability.

3.3 Fourier Transform Infrared Spectroscopic Studies

Chemical changes, which occur in the polymer during the aging process, were followed by IR spectroscopy. Fourier transform-infrared spectroscopy results show the increase of carbonyl (-C=O) and hydroxyl (-O-H) functional groups on the surface of aged PM1 sample. This result suggests that hydrocarbon groups locally undergo the oxidation on the surface of the sample due to UV photo-oxidation and chemical oxidation by ozone. Figure 2 (A) and 2 (B) show FTIR spectra of samples as a function of ozone aging time. Figure 2 (C) and 2 (D) show FTIR spectra of UV-aged samples. The most significant changes in the IR spectra were carbonyl (1785-1700 cm^{-1}) for both aging treatments. The IR spectrum of the samples was

followed in the range of 1710 – 1735 cm^{-1}. As seen in Figures 2 (A) and (B), during the early stage of the ozone aging process, the species that were present a composite absorbance in which aldehyde (1735 cm^{-1}) and ketone (1714 cm^{-1}) are the main species. The absorption band that is assigned to the ketone stretch band (1714 cm^{-1}) increased in intensity and broadened with aging time, which indicates the presence of more than one oxidation product. At a later stage of aging, the peak corresponding to carboxylic acid (1710 cm^{-1}) increased as seen in Figure 2 (B). The presence of carboxylic acid is indicative of chain session of LDPE. The carbonyl band is a result of overlapping of various stretching vibration bands including those of aldehyde, esters (1733 cm^{-1}), ketones, carboxylic acid groups and g lactones (Lin, 1997; Khabbaz et al., 1998; Setnescu et al., 1998; Tavares et al., 2003; Roy et al., 2007). As seen Figure 2 (C) and (D), for UV aged samples, the peak corresponding to ketone stretch band at 1716 cm^{-1} increases due to the formation of different oxidation products by UV oxidation. The height increase of peaks at 2360 and 2340 cm^{-1}, which correspond to carbon dioxide (Lefohn et al., 1998), indicates the oxidation of the polymer by the UV aging process. Additionally, the peaks at 1462 and 1377 cm^{-1} corresponding to methyl and methylene deformation became clearer and larger over time for the UV aging (Larkin, 2001). In particular, for PM2 sample, CO stretching at 1077 and 1048 cm^{-1} was observed (Coelho et al., 2015). During the UV aging, the height increased over time due to UV oxidation of PE. Based on the results of TGA in Section 3.2, it seems that UV photo-oxidation mainly occurs on the surface of polymer films and then UV could reach the inside of films through defects due to UV oxidation for PM1 sample. However, in the case of PM2 sample, the photo-oxidation occurred on their surface only and its thermal stability was improved, indicating the higher amounts of nanoclay particles in PM2 than PM1, resulting in higher stability via UV photo-oxidation.

Moreover, results of the carbonyl index (CI) calculated by taking the ratio of the intensity of absorbance signals at 1740:2020 cm^{-1} are plot as a function of ozonation time (see Supplemental Figure S4). The PM1 sample showed changes in CI values with increase in ozone exposure time, but the changes of CI values for PM2 sample were significantly larger than PM1. The results agree with the previous study that polyethylene films enter into the decay stage at CI greater than 6 (Roy et al., 2008).

3.4 X-Ray Diffraction (XRD) Analysis

XRD was used to investigate the structure of clay-containing composites and the kinetics of polymer melt intercalation. By monitoring the position, shape and intensity of the basal reflections from the distributed clay particles, the structure of the nano-clay composite–intercalated or exfoliated can be identified. XRD patterns of samples shown in Figure 3 (A) and 3 (B) display structural changes occurred when PM1 and PM2 films were exposed to UV light at different durations, respectively. Clear peaks at a range of 4–8 of 2θ for PM2 indicate more nanoclay was added in the sample. However, the peaks were not detected in PM1 and it seems that the quantity of nanoclay in PM1 is lower than a detection limit of the detection method. X-ray diffraction was significantly decreased, indicating a decrease in crystallinity of samples and loss of nanoclay from the samples due to decomposition of samples by oxidation and chain scission during aging processes. XRD data of the products obtained show an inter-gallery spacing varying from 30 to 43 Å. There is a noticeable

increase of the 9.6 Å basal plane spacing of Na-montmorillonite, and from the spacing in the virgin organically-modified clay, which is about 17 Å indicating that the polymer and clay form a nanocomposite. The intercalated form of the nanocomposite in which the gallery spacing has increased to accommodate the polymer has been produced in this study (Dadblin et al., 2008; Andersson, 2010). The possibility of delamination was confirmed with Scanning electron microscopic (SEM) examination. Exfoliation existed in the LDPE-nano-clay systems, which clay layers have fractured and dispersed evenly into the polymer matrix. This resulted from higher mobility and freedom of amorphous chain for further crystallization due to the chain session by photo-oxidation because the degradation happens simultaneously at multiple positions (Guadagno et al., 2001). Full spectrum X-ray analysis of PM1 and PM2 samples shows little difference (Supplemental Figure S5).

3.5 Atomic Force Microscopy (ATM) and Scanning Electron Microscopy

AFM images are used to analyze changes in structural parameters of thin films. AFM measurements on the unaged samples provide that the sample surfaces that are very even and they did not show any elevated surface features in the range of a few nanometer as seen in Figure 3 (C) and 3 (D). From the half-width of the XRD profile peaks of the thin films, the crystal size of the particles was determined to be around 14 nm. These results are in agreement with the AFM images of thin films. The surface roughness (Ra) with a value less than 30 nm confirms that flatness and homogeneity of pristine LDPE film. The average roughness Ra is defined by:

$$R_a = \frac{1}{N} \sum |Z_i - Z|$$

At which N is the number of pixels, Z the average height value and Z_i the height value at position i. After aging of the samples of PM1 and PM2 under UV irradiation for 100 hr, the topography of the samples revealed elevated surface features with a surface roughness of 178 nm for PM2 and only 38 nm for PM1 as shown in Figure 3 (E) and 3 (F). There is a striking difference between the surface structures of two samples. The change in average roughness for PM1 and PM2 were 43% and 450%, respectively. The roughness was increased by a factor of ten for PM2 sample after four days of irradiation. Although cracks were observed on the surface of UV aged PM1 in SEM images (Supplemental Figure S6) compared to PM2 (Supplemental Figure S7), the detailed AFM analysis indicates the surface of both UV aged PM1 and PM2 samples can be easily damaged by photo-oxidation.

3.6 Measuring Released Nano-clay Particles

3.6.1 Transmission Electron Microscopy (TEM) of released particles—

Nanoparticle released to the wash-water from aged nanoclay enforced LDPE samples were dried imaged using a high resolution-TEM, following methods established by group of researchers (Wohlleben et al., Carbon, 2017). The high resolution-TEM images obtained were analyzed using an image processing program (ImageJ software, US NIH). Figures 4 (A) and (B) show TEM images of unaged composite. Figures 4 (C) and (D) demonstrate clay nanoparticles released, where the clay particles are dark in a matrix of plate-like montmorillonite that consists of ~ 1 nm thick aluminosilicate layers surface-substituted with

metal cations: individual clay layers and agglomerates consisting of three or more stacked layers were observed. Figure 4 (E) and (F) show TEM micrographs of stacked nano-clay layers, which released from the polymeric matrix. The layers are uniformly spaced with an observed average interlayer distance of 2 to 4 nm. The measured size of released nano-clay particles ranged from 2 to 8 nm. These results of high resolution -TEM analysis confirmed that nano-clay particles were leached from the polymer films due to the oxidation during UV and ozone aging processes. Interestingly, large particles (> 100 μm) were observed in the samples. Based on the results of EDS analysis as seen in Supplemental Figure S9, are similar to TiO_2 particles, which may be the additive to prepare PM1 films.

3.6.2 Measuring Released Nano-clay Particles Using ICP-AES—The mass of the main elements contained in PM1 and PM2 samples as obtained from the ash of pyrolyzed samples (Supplemental Figure S8 shows). Both samples contain the same types of elements. These results are comparable with the energy dispersive X-ray spectroscopy analysis of samples of LDPE clay composite and LDPE samples (Supplemental Figure S9). The total content of metals and other elements detected by ICP-AES for PM1 and PM2 film was 0.18–0.30 and 0.16–0.23% w/w, respectively. After the UV or ozone aging, the concentration of metals and other elements for PM1 and PM2 samples was determined by ICP-AES (see Figures S10 (A)–(D)). For UV aged PM1 and PM2 samples (Figure S10 (A)), the released mass of each element for PM1 was much larger than PM2, indicating PM1 was degraded more than PM2 sample. This result is in agreement with TGA result (Figures 1 (B) and (C)) showing lower thermal stability of PM1 due to the high degree of photo-oxidation because of a low content of nano-clays. As seen in Figure S10 (A), the mass of Fe in PM2 sample is much higher than PM1. It seems that nano-clay mainly contains Fe. However, as seen in Figure S10 (B), the released mass of each element except for Fe is similar for both ozone aged PM1 and PM2 samples. Because ozone can easily penetrate the polymer films when damaged by ozone, no significant improvement of film stability by the addition of nano-clay was found. As shown in Figure S10 (D), the released mass of elements for ozone aged samples was much higher than UV aged samples, almost 10 times higher. It indicates that chemical oxidation by ozone is more powerful than UV photo-oxidation because the photo-oxidation is a surface-limited reaction.

3.6.3 Measuring nano-clay particles induced oxidative stress—The released nano-clay particles and their effect on generating singlet oxygen, ($^1O_2$) were determined with an indirect method using a fluorescent sensor named Singlet Oxygen Sensor Green (SOSG). Figure 5 (a) show that as UV dosage increased, the intensity of SOSG for all samples with different nano-clay concentrations increased, indicating that released nano-clays produced $^1O_2$ under UV illumination. Since iron contained in the nano-clays is a transition metal, it can produce ROS by participating in reactions of one-electron oxidation–reduction (Yin et al., 2012). Iron oxides are usually used as photocatalysts to decompose different pollutants in water (Karunakaran and Senthivelan, 2006; Zhang et al., 2014; Liu et al., 2015;). Interestingly, the formation of $^1O_2$ decreased at higher concentration of nano-clays. It seems that only a limited amount of SOSG fluorescent added into the test reactor was utilized to form $^1O_2$ due to adsorption of SOSG onto nano-clays. Also, the light utilization of nano-clays may not be efficient during the reaction due to increased light

scattering by the presence of large amount of nanoclay particles in water. Based on the results of the measurement of SOSG intensity of nano-clay standards (i.e., a calibration curve for indirect nanoclay quantification), the released nano-clay was estimated from aged composites. As shown in Figure 5 (b), the SOSG intensity for the released sample was larger than 5 mg L^{-1} nano-clay but smaller than 1 mg L^{-1} nano-clay. The estimated concentration of released nano-clays from the aged LDPE nanocomposite was about 1 mg L^{-1}. These results of singlet oxygen measurement using SOSG fluorescent confirmed the release of clay nanoparticles from the LDPE nanocomposite, resulting from damages by photo-oxidation during the aging processes along with the results of DLS, TEM and ICP analyses. Even though the release of clay nanoparticles is effectively investigated with the indirect quantification method, the accuracy of the method is not very high. Unfortunately, nanoclays isolated by LDPE in the composites could not be involved in ROS production under UV illumination, resulting in underestimation of the released nanoclays. However, the method might be a useful technique for indirectly quantifying released nanoclay particles from aged polymer composite.

3.6.4 Toxicity of Released Nano-clay Particles—Considering that inhalation maybe a primary route for degraded nanoparticles, the toxic behavior of PM1 and PM2 was tested in A549 alveolar epithelial cells. Two types of cellular toxicity studies were performed. The first test investigated whether the particles induced activation of intracellular ROS. In the presence of intracellular ROS, the cells convert H2DCF (2′,7′-dichlodihydrofluorescein) to fluorescent DCF. The assay was tested using the positive control, Sin-1, which generates both superoxide ions and nitric oxide that spontaneously form peroxynitrite, a potent oxidant. Figure 6 (A) showed that the assay worked by producing fluorescent DCF in the presence of Sin-1, and that these levels were significant from all other treatments. PM1 and PM2 did not produce ROS, as levels of fluorescence were comparable to untreated cells. The second test assessed the cells activity and viability, using the MTS assay, upon exposure to the various treatment groups. MTS, a tetrazolium compound, is bioreduced by cells into formazan, a colored product that can be detected by optical density. $CdSO_4$ was used as the positive control, and Figure 6 (B) shows that $CdSO_4$ significantly decreased the activity and viability of cells ($p < 0.001$), compared to all other treatment groups. Once again, PM1 and PM2 were comparable to untreated cells for both the 24 h and 48 h time points. The concentrations of PM1 and PM2 were tested at the highest concentration, which allowed us to conclude that these products did not show significant levels of toxicity. The reduced toxicity of clay nanomaterials was not a surprising finding to the authors as anionic clay material as anionic surfaces are negatively charged and thus cannot engage as readily to the negatively-charged cell-surface. Previous studies have also concluded that clay based nanoparticles have lower toxicity risk (Al-Awady et al., 2015; Choi et al., 2009). Nevertheless, particle size, the shape of the nanomaterial, and other surface properties may also contribute to the reduced toxicity levels of clay-nanoparticles.

4. Conclusion

This study has shown there is strong evidence that the stability of two types of food packaging LDPE films are altered when exposed to environmental conditions, UV-

irradiation or ozone in the presence of moisture. Both LDPE samples underwent oxidative degradation during UV irradiation or ozone exposure resulting in a substantial change in physical, structural, and thermal properties. The rate of property changes for PM2, containing a larger amount of nano-clays, was higher than that observed in PM1. This suggests that clay mineral oxide ions present in nano-clays of PM2 accelerate the photo-oxidation degradation more than PM1. Various tests have shown that the presence of nano-clay accelerated in degradation of the LDPE and enhanced the release of clay particles. Although aging models have a limited use for practical applications because real life aging conditions are usually far more complex than controlled experimental conditions in laboratory, this and previous studies have showed the high volume of nanocomposite that is used for non-structural applications such as food packaging and the nanomaterials could be released in the course of life cycle and risk human health and the environment. The results of this study clearly show that the release of nanomaterials from composites. Therefore, the selection of environmentally friendly nanofillers in nanocomposites is very critical to protect the health of humans, animals and the environment.

Supplementary Material

Refer to Web version on PubMed Central for supplementary material.

Acknowledgments

Disclaimer

The views expressed in this manuscript are those of the authors and do not necessarily represent the views or policies of the U.S. Environmental Protection Agency. CH is a postgraduate research participant at the National Risk Management Research Laboratory administered by the Oak Ridge Institute for Science and Education through an interagency agreement between the U.S. Department of Energy and the U.S. Environmental Protection Agency.

References

Al-Awady MJ, Greenway GM, Paunov VN. Nanotoxicity of polyelectrolyte-functionalized titania nanoparticles towards microalgae and yeast: role of the particle concentration, size and surface charge. RSC Adv. 2015; 5:37044–37059.

Amin MU, Scott G. Photo-initiated oxidation of polyethylene effect of photo-sensitizers. Eur Polym J. 1974; 10:1019–1028.

Andersson, C. Composite laminates: Properties, performance and applications. Doughett, A., Asnarez, P., editors. Nova Science Publishers, Inc.; New York, NY: 2010. p. 83-119.

Azeredo HMC. Nanocomposites for food packaging applications. Food Res Int. 2009; 42:1240–1253.

Castro CA, et al. Photocatalytic production of $^1O_2$ and OH mediated by silver oxidation during the photoinactivation of Escherichia coli with TiO_2. J Hazard Mater. 2012; 211–212:172–181.

Chen W, et al. Enhanced mechanical properties and morphological characterizations of poly(vinyl alcohol)-carbon nanotube composite films. Applied Surface Science. 2005; 252:1404–1409.

Chidambaram M, Krishnasamy K. Drug-drug/drug-excipient compatibility studies on curcumin using non-thermal method. Adv Pharm Bull. 2014; 4:309–312. [PubMed: 24754017]

Choi S, Oh J, Choy J. Toxicological effects of inorganic nanoparticles on human lung cancer A549 cells. J Inorganic Biochem. 2009; 103:463–471.

Coelho GR, et al. Antiviral action of hydromethanolic extract of geopropolis from *Scaptotrigona Postica* against Antiherpes Simplex Virus (HSV-1). Evidence-Based Complementary and Alternative Medicine. 2015; 2015:296086. [PubMed: 25861357]

Cohen, SH., Bray, MT., Lightbody, ML. Atomic force microscopy/scanning tunneling microscopy. New York: Plenum Press; 1994.

Dadblin S, Nofersti M, Frounchi M. Oxygen barrier LDPE/LLDPE/organoclay nano-composite films for food packing. Macromol Symp. 2008; 274:22–27.

Davoodi MG, Sourki AH. Influence of environmental conditions on permeability of low density polyethylene/clay nano composites used in bread packaging. Int J Biosci. 2014; 5:12–15.

Giannelis EP. Polymer layered silicate nanocomposites. Adv Mater. 1996; 8:29–35.

Grassi, N., Scoot, G. Polymer degradation and stabilization. Cambridge University Press; Cambridge, UK: 1985.

Guadagno L, et al. Chemical and morphological modification of irradiated linear low density polyethylene (LLDPE). Polym Degrad Stab. 2001; 72:175–186.

Guo YY, et al. Cytotoxic and genotoxic effects of multi-wall carbon nanotubes on human umbilical vein endothelial cells in vitro. Mutat Res Genet Toxicol Environ Mutagen. 2011; 721:184–191.

He W, et al. Unraveling the enhanced photocatalytic activity and phototoxicity of ZnO/metal hybrid nanostructures from generation of reactive oxygen species and charge carriers. *ACS Appl. Mater.* Interfaces. 2014; 6:15527–15535.

Hinsken H, et al. Degradation of polymers during melt processing. Polym Degrad Stabil. 1991; 34:279–293.

ICDD. The International Centre for Diffraction Data. 1997–2017. www.icdd.com accessed on March 11, 2017

Ju L, et al. Proteomic analysis of cellular response induced by multi-walled carbon nanotubes exposure in A549 cells. PLoS One. 2014; 9:e84974. [PubMed: 24454774]

Karunakaran C, Senthivelan S. Fe2O3-photocatalysis with sunlight and UV light: Oxidation of aniline. Electrochem Commun. 2006; 8:95–101.

Khabbaz F, Albertsson AC, Karlson S. Trapping of volatile low molecular weight photoproducts in inert and enhanced degradable LDPE. Polym Degrad Stabil. 1998; 61:329–342.

Kim JY, et al. Effect of Modified carbon nanotube on the properties of aromatic polyester nanocomposites. Polymer. 2008; 49:3335–3345.

Kocun M, Grandbois M, Cuccia LA. Single molecule atomic force microscopy and force spectroscopy of chitosan. Colloids Surf B Biointerfaces. 2011; 82:470–476. [PubMed: 21071189]

Larkin, PJ. IR and Raman spectroscopy: Principles and spectral interpretation. Waltham, MA: Elsevier; 2011.

LeBaron PC, Wang Z, Pinnavaia TJ. Polymer-layered silicate nanocomposites: an overview. Appl Clay Sci. 1999; 15:11–29.

Lefohn AE, Mackie NM, Fisher ER. Comparison of films deposited from pulsed and continuous wave acetonitrile and acrylonitrile plasmas. Plasmas Polym. 1998; 3:197–209.

Lewicka ZA, et al. Photochemical behavior of nanoscale TiO_2 and ZnO sunscreen ingredients. J Photochem Photobiol A. 2013; 263:24–33.

Lin LH, Yu NK. Morphology and thermal properties of poly(L-lactic acid)/organoclay nanocomposites. J Appl Polym Sci. 2007; 106:260–266. 2007.

Lin Y. Study of ultraviolet photoxidative degradation of LDPE film containing cerium carboxylate photosensitizer. J Appl Poly Sci. 1997; 63:811–818.

Liu X, et al. Facile synthesis of porous Fe_2O_3 nanorods and their photocatalytic properties. J Soudi Chem Soc. 2015; 19:479–484.

Manchado ML, et al. Thermal and mechanical properties of single-walled carbon nanotubes–polypropylene composites prepared by melt processing. Carbon. 2005; 43:1499–1505.

Mark, HF. Encyclopedia of Polymer Science and Technology. 3rd. John Wiley & Sons; 2004.

Morgan AB. Nanoclays for Composites. Material Matters. 2007; 2:20–25.

Moniruzzaman M, Karen IW. Polymer nanocomposites containing carbon nanotubes. Macromolecules. 2006; 39:5194–5205.

Paul MA, et al. (Plasticized) polylactide/(organo-)clay nanocomposites by in situ intercalative polymerization. Macromole. Chem Phys. 2005; 206:484–498.

Roy PK, et al. Studies on the photo-oxidative degradation of LDPE films in the presence of oxidized polyethylene. Polym Degrad Stab. 2007; 92:1151–1160.

Roy PK, et al. Degradation behavior of linear low-density polyethylene films containing prooxidants under accelerated test conditions. J Appl Polym Sci. 2008; 108:2726–2733.

Schlagenhauf L, et al. Carbon Nanotubes Released from an Epoxy-Based Nanocomposite: Quantification and Particle Toxicity. Environ Sci Technol. 2015; 49:10616–10623. [PubMed: 26251010]

Setnescu R, Jipa S, Osawa S. Chemiluminescence study on the oxidation of several polyolefins. I. Thermal induced degradation of additive-free polyolefins. Polym Degrad Stab. 1998; 60:377–383.

Shemesh R, et al. LDPE/clay/carvacrol nanocomposites with prolonged antimicrobial activity. J Appl Polym Sci. 2015; 132:41261.

Singh B, Sharma N. Mechanistic implications of plastic degradation. Polym Degrad Stabil. 2008; 93:561–584.

Siročić AP, et al. Development of low density polyethylene nanocomposites films for packaging. Polymer Bulletin. 2014; 71:705–717.

Tavares AC, et al. The effect of accelerated aging on the surface mechanical properties of polyethylene. Polym Degrad Stabil. 2003; 81:367–373.

Vaia RA, et al. Microstructural evolution of melt intercalated polymer-organically modified layered silicates nanocomposites. Chem Mater. 1996; 8:2628–2635.

Yin J-J, et al. Dual role of selected antioxidants found in dietary supplements: Crossover between anti- and pro-oxidant activities in the presence of copper. J Agric Food Chem. 2012; 60:2554–2561. [PubMed: 22339379]

Wohlleben W, Neubaue N. Quantitative rates of release from weathered nanocomposites are determined across 5 orders of magnitude by the matrix, modulated by the embedded nanomaterial. 2016; 1:39–45.

Wohlleben W, et al. NanoRelease: Pilot interlaboratory comparison of a weathering protocol applied to resilient and labile polymers with and without embedded carbon nanotubes. Carbon. 2017; 113:346–360.

Zhang X, et al. Improvement of Hematite as Photocatalyst by Doping with Tantalum. *J. Phys. Chem.* C. 2014; 118:16842–16850.

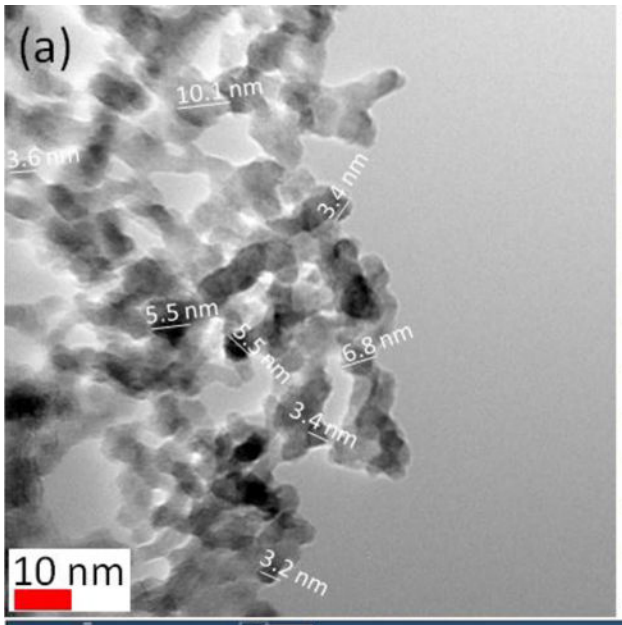

(b)	Area 1	Area 2	Area 3	Area 4	Area 5	Average
Element	wt%	wt%	wt%	wt%	wt%	wt%
O	36.13	39.04	37.11	35.74	26.29	34.86 ± 4.44
Mg	0.62	0.57	0.6	0.68	0.64	0.62 ± 0.04
Al	25.73	20.01	23.46	26.26	40.57	27.21 ± 7.04
Si	7.5	7.8	7.79	7.81	7.72	7.72 ± 0.12
K	0.07	0.04	0.07	0.07	0.09	0.07 ± 0.02
Ca	0.16	0.19	0.16	0.15	0.16	0.16 ± 0.01
Ti	17.25	18.71	17.96	17.2	14.06	17.04 ± 1.59
Fe	8.76	9.57	8.92	8.44	7.34	8.61 ± 0.73
Zn	3.78	4.06	3.92	3.65	3.13	3.71 ± 0.32
Total	100	100	100	100	100	

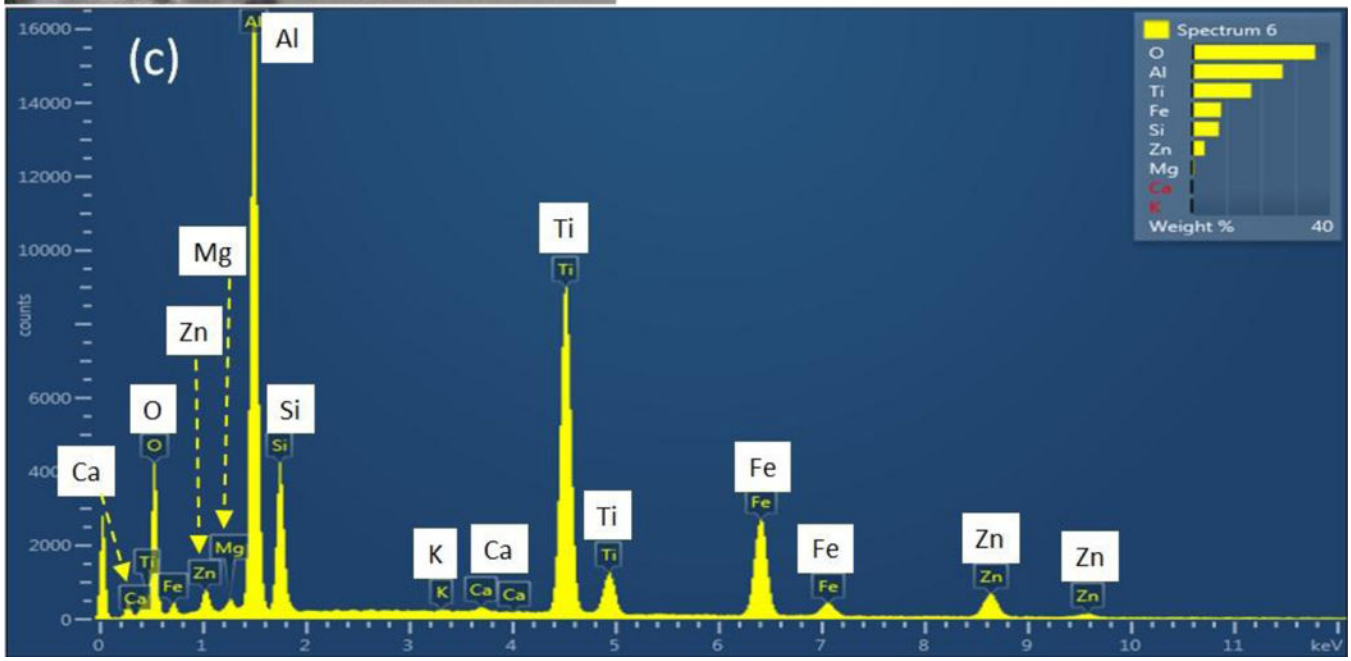

Figure 1.

Thermogravimetric analysis of nano-clay composite packaging materials (A) pristine PM1 and PM2 samples, and (B) UV aged PM1 and (c) UV aged PM2 samples.

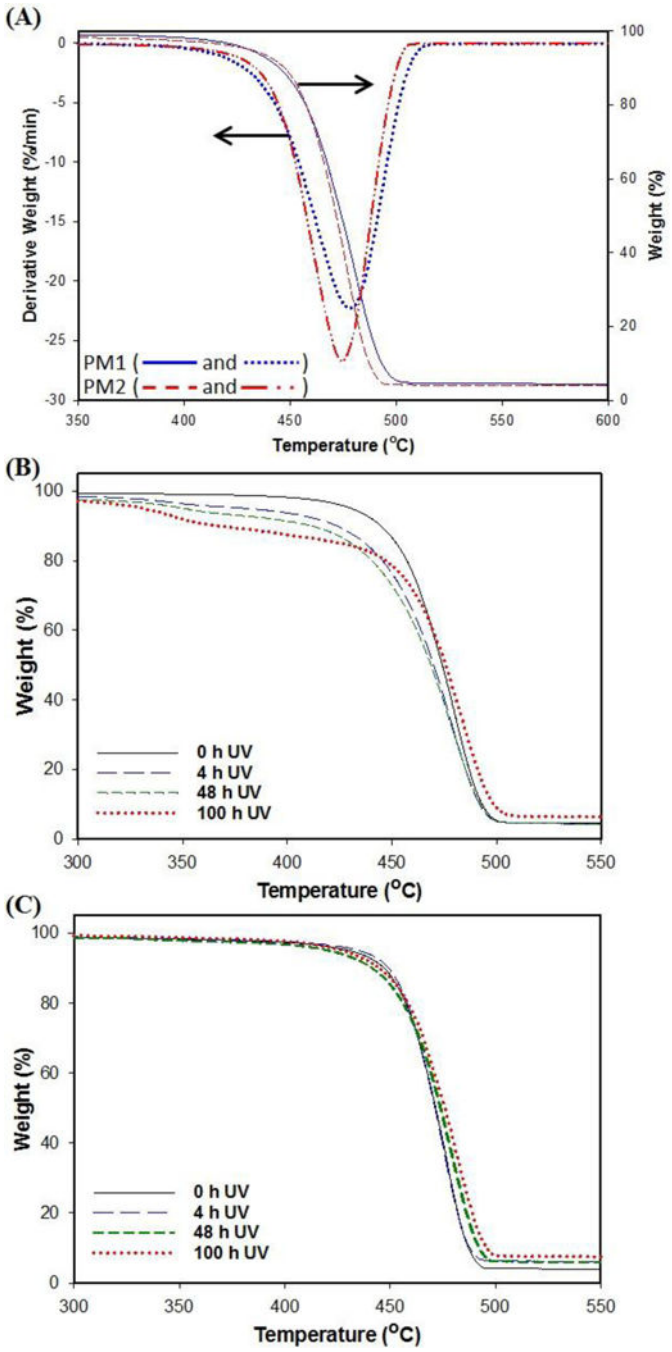

Figure 2.

Fourier transfer infrared spectrum analysis of aged packaging materials (A) PM1 and (B) PM2 samples, and UV-aged (C) PM1 and (B) PM2 samples with different aging times.

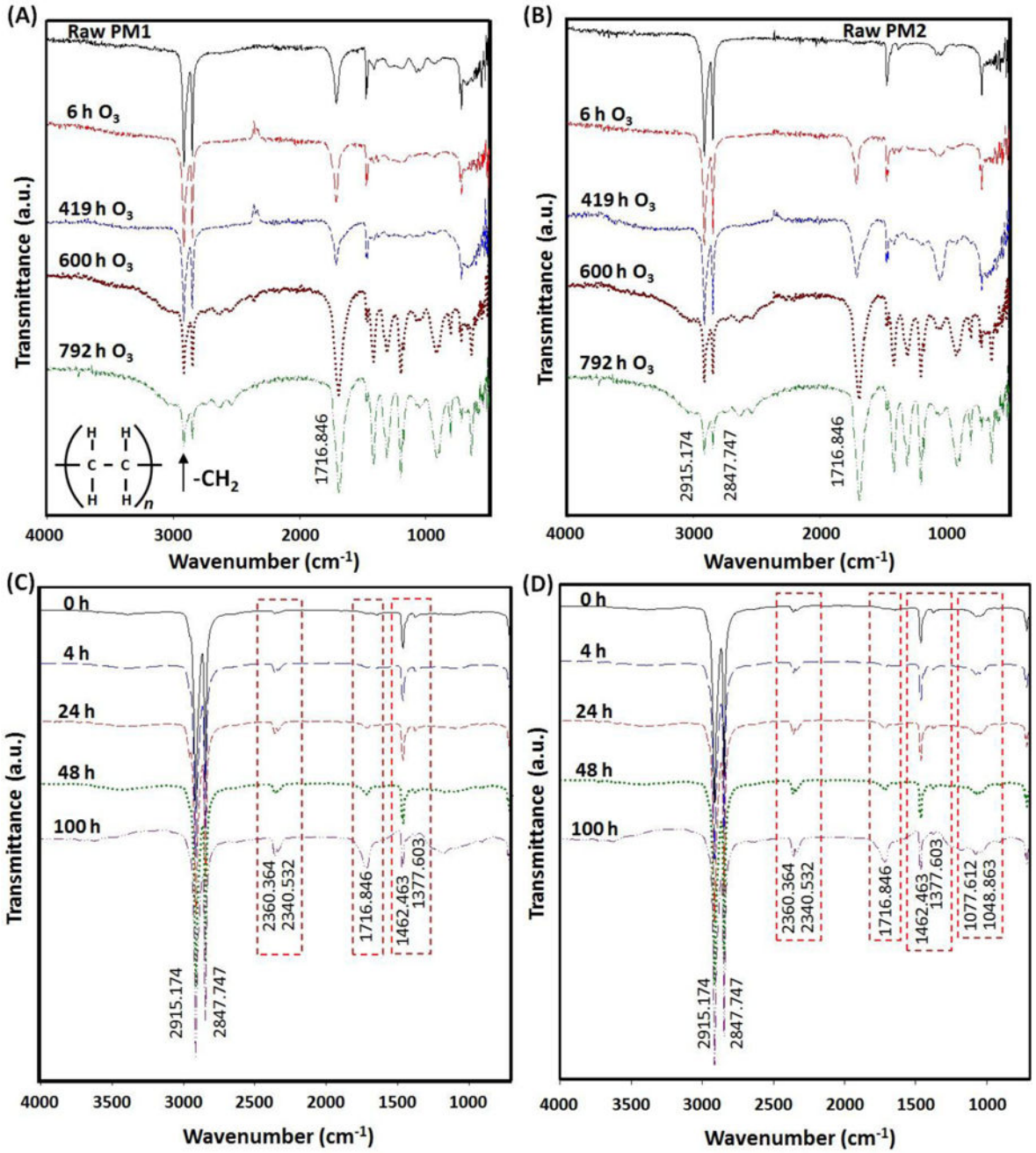

Figure 3.

Low angle X-ray diffraction patterns of (A) PM1 and (B) PM2 samples, and atomic force microscopic images of PM1 (C) and (D), and PM2 (E) and (F) after UV accelerated aging.

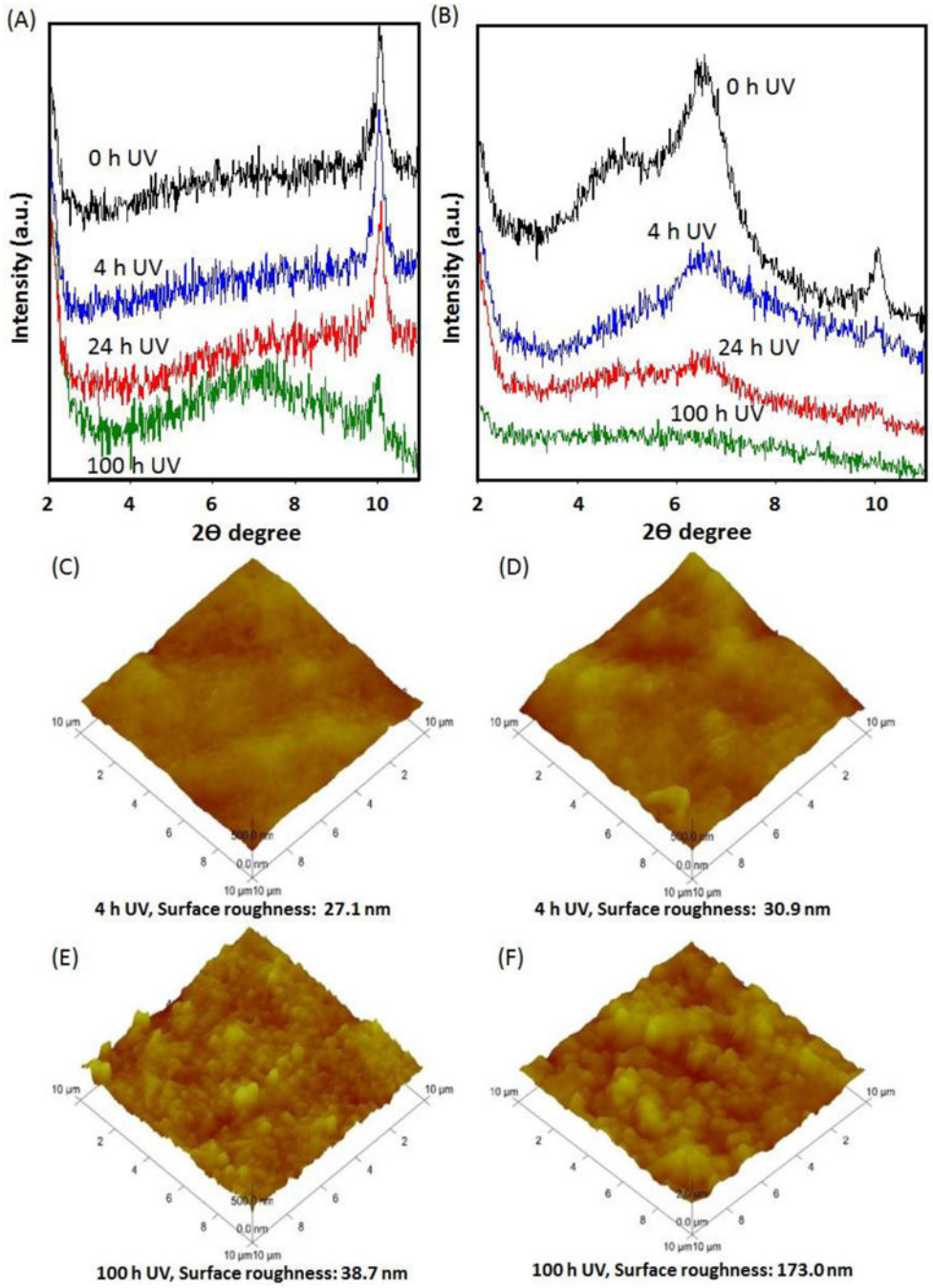

Figure 4.

High resolution transmission electron microscopy images of released nanoparticles from PM2 samples after 100 h of UV aging (A) and (C), and 800 h of O_3 aging (B) and (D).

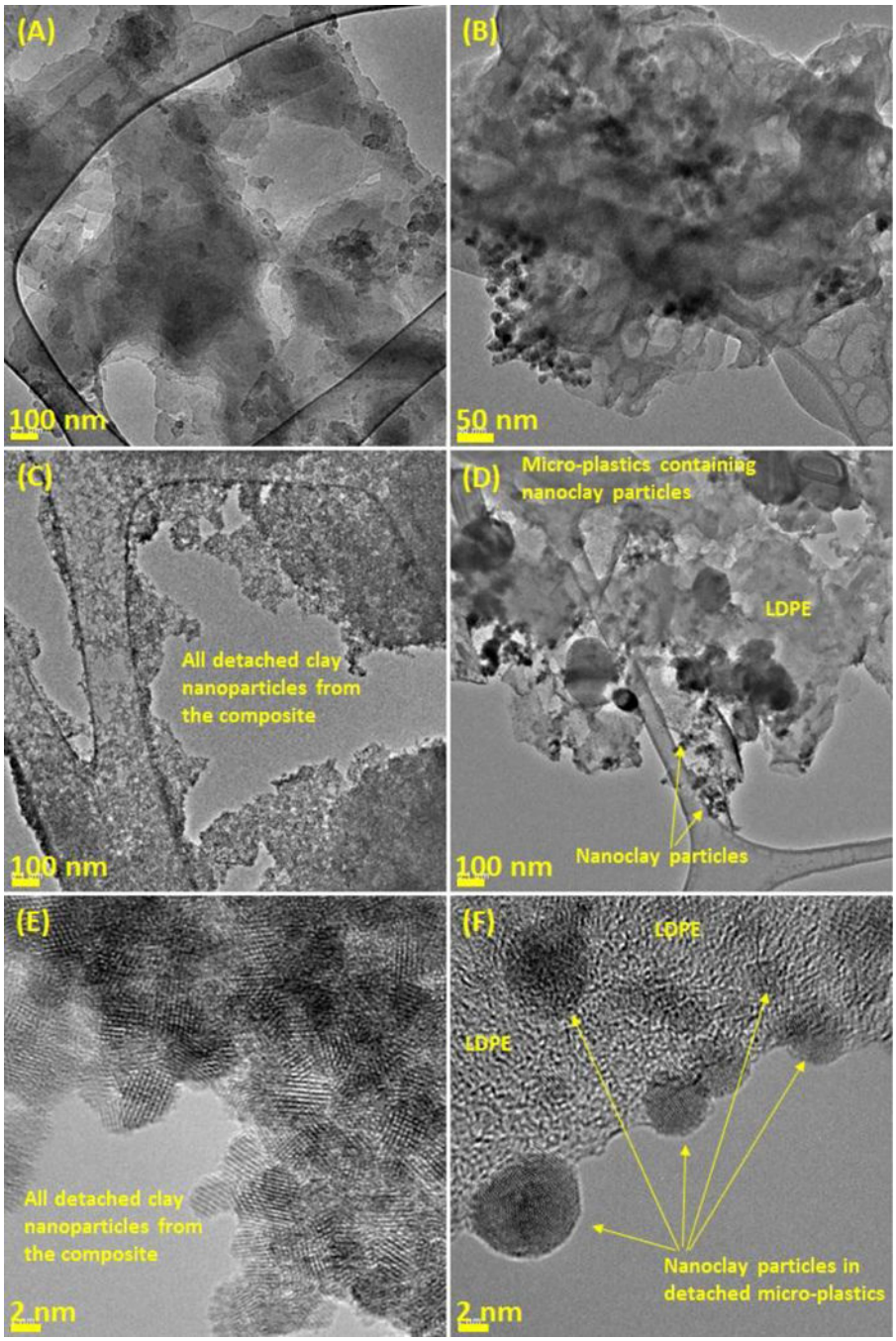

Figure 5.

The measurement of reactive oxidative species (ROS) formation of released nano-clay particles from UV aged PM2 by measuring fluorescent detection reagent, SOSG: (a) Intensity changes of SOSG over UV irradiation time and (b) Averaged intensity of SOSG with different concentrations of nano-clays and a released sample at 30 min UV illumination.

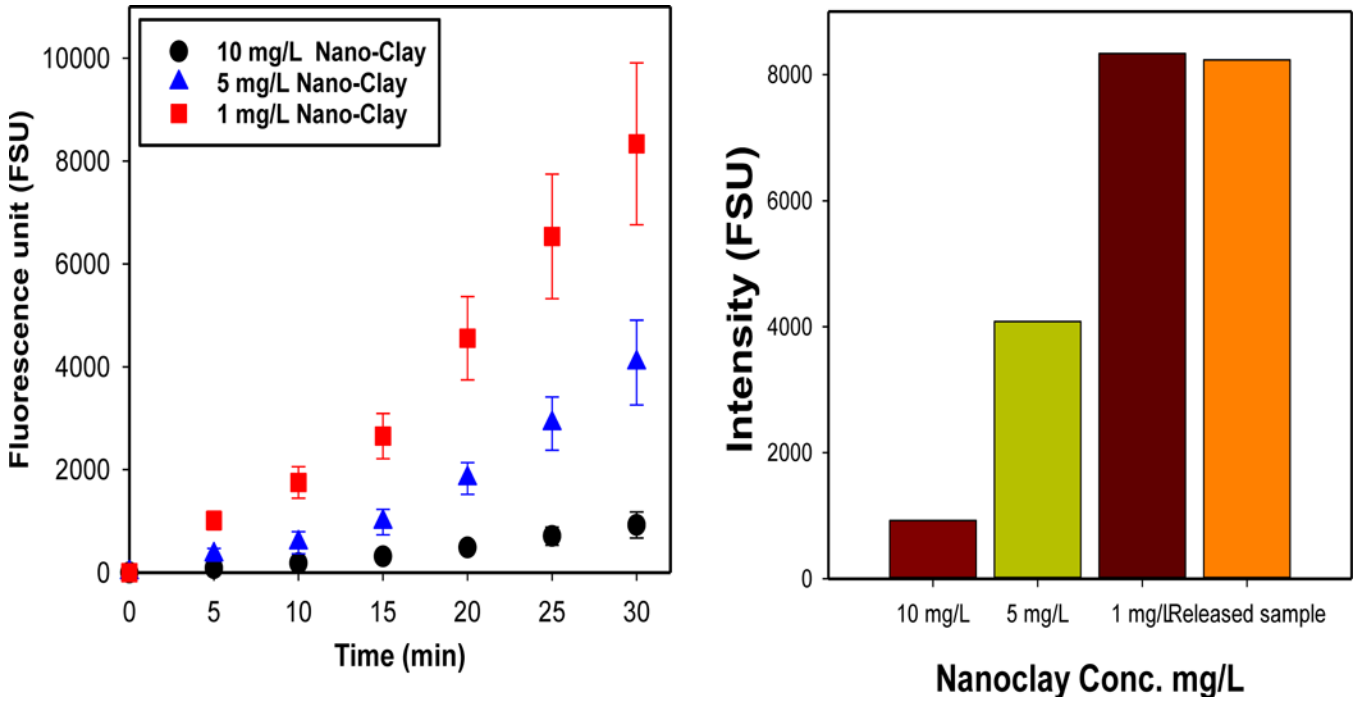

Figure 6.

Intracellular ROS generation and cell activity responses to PM1 and PM2. (A) Production of ROS as measured in A549 cells after exposure to Sin-1 (positive control), PM2, PM1, and no treatment (untreated cells). Intracellular ROS generation was determined by increased DCF fluorescence. * p <0.001 compared to positive control. (B) Cell activity and viability as determined by the quantity of production of formazan, using the MTS Assay. A549 cells were exposed to $CdSO_4$, PM2, PM1, and no treatment (untreated cells), for 24 and 48 h. * p <0.001 compared to positive control.

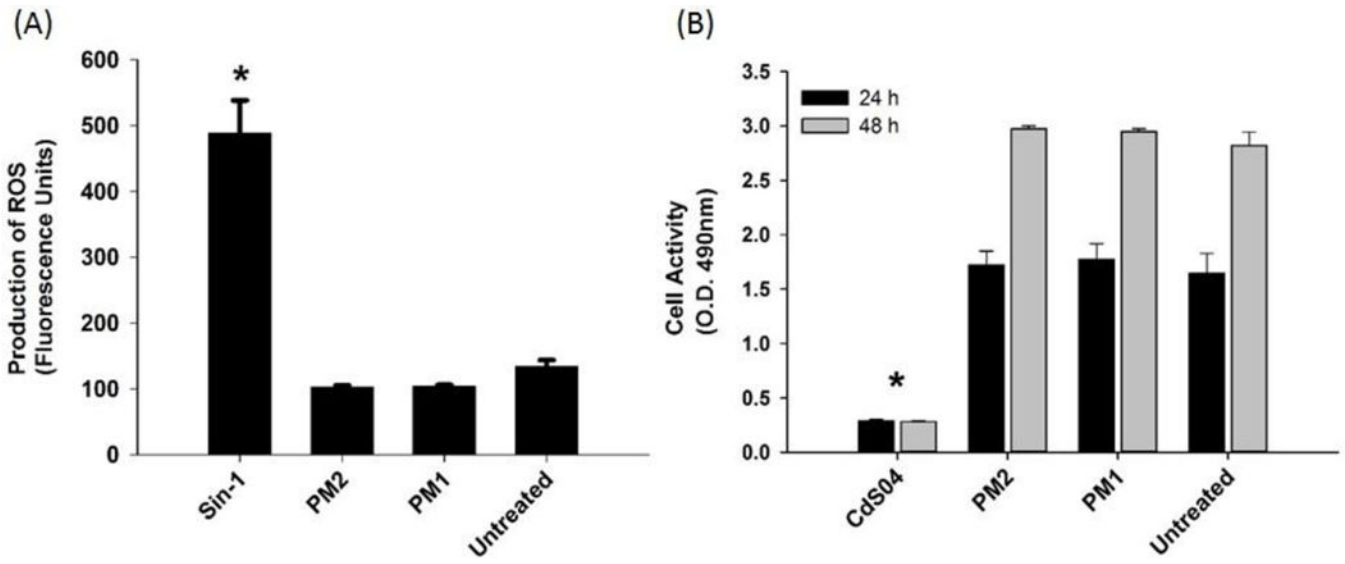

Figure 7.

Intracellular ROS generation and cell activity responses to PM1 and PM2. (A) Production of ROS as measured in A549 cells after exposure to Sin-1 (positive control), PM2, PM1, and no treatment (untreated cells). Intracellular ROS generation was determined by increased DCF fluorescence. * $p < 0.001$ compared to positive control. (B) Cell activity and viability as determined by the quantity of production of formazan, using the MTS Assay. A549 cells were exposed to $CdSO_4$, PM2, PM1, and no treatment (untreated cells), for 24 and 48 h. * $p < 0.001$ compared to positive control.